ELSEVIER

Polymer 44 (2003) 743–756

polymer

www.elsevier.com/locate/polymer

Solid state structure–property behavior of semicrystalline poly(ether-*block*-amide) PEBAX® thermoplastic elastomers

Jignesh P. Sheth, Jiannong Xu[1], Garth L. Wilkes*

Polymer Materials and Interfaces Laboratory, Department of Chemical Engineering, Virginia Polytechnic Institute and State University, Blacksburg, VA 24061-0211, USA

Received 19 June 2002; received in revised form 22 October 2002; accepted 23 October 2002

Abstract

The solid state structure–property behavior was investigated of a series of poly(ether-*block*-amide) PEBAX® thermoplastic elastomers based on nylon 12 and poly(tetramethylene oxide) with varying hard segment content. Particular emphasis was placed on better defining the morphological features of this entire series of commercially available materials. Compression molded and solution cast samples were studied by the techniques of DMA, DSC, WAXS, SAXS, AFM, SALS and stress–strain response. The strain-induced crystallization behavior of the soft polyether (PE) segments was also investigated. All samples exhibited a microphase separated morphology over a broad temperature range. As expected, an increase in the interconnectivity of the polyamide hard phase was greatly controlled by the polyamide (PA) content. Due to the crystallization of the PA hard segment, the formation of PA lamellar crystals was noted in both melt and solution cast films. At the higher PA contents, a distinct spherulitic superstructure was also observed but this form of morphological texture was diminished as the PE soft segment content increased. Limited studies of the deformation/recovery behavior of the spherulitic superstructure provided further information concerning the interaction between the hard and soft segments.

Keywords: Poly(ether-*block*-amide); Block copolymer; Strain-induced crystallization

1. Introduction

Thermoplastic elastomers (TPE) are block copolymers where thermodynamic incompatibility between the two blocks typically leads to a microphase separated morphology. Furthermore, at the normal service temperatures one block acts as the hard phase and the other acts as the soft phase. The hard phase generally exists below its glass transition temperature, T_g, or in certain cases its melting temperature, T_m, if there is enough crystallinity to promote a hard phase. The soft phase on the other hand has its T_g (or T_m if the soft block can crystallize) lower than the normal service temperature. Covalent links between the two chemically different blocks prevent macrophase separation. Thus, depending upon the relative amounts of the hard and the soft blocks, the glassy (or crystalline) phase of the hard block acts as a physical cross-link site for the rubbery phase of the soft block. TPEs have also been called 'virtually cross-linked' elastomers by Scollenberger [1,2] who was the first to report that linear segmented ester-based thermoplastic polyurethanes exhibited high extensibility and elasticity in an unvulcanized form and yet behaved in their service temperature range as cross-linked elastomers.

At elevated temperatures, the hard block also softens (or melts) enabling these TPEs to be processed as thermoplastics. Due to the inherent flexibility afforded by their chemistry, block or segment molecular weight, and relative amounts of the hard and soft blocks, the properties of such materials can be tailored to suit a wide range of application requirements. Good elastomeric properties, a broad service temperature range, and in many cases excellent resistance to chemical and thermal aging has allowed TPEs to replace many earlier chemically cross-linked materials in several commercial applications and in some instances has helped create completely new ones.

Thermoplastic polyurethanes (TPU), a sub-category of TPEs, were one of the first to be made commercially available. In the United States, TPUs were marketed for the first time in the 1960s by Goodrich, Mobay and Upjohn

* Corresponding author. Tel.: +1-540-231-5498; fax: +1-540-231-9511.
E-mail address: gwilkes@vt.edu (G.L. Wilkes).
[1] Present address: Milliken Chemical, M-401, Division of Milliken and Company, 920 Milliken Road, P.O. Box 1927,Spartanburg, SC 29304, USA.

0032-3861/03/$ - see front matter © 2002 Elsevier Science Ltd. All rights reserved.
PII: S0032-3861(02)00798-X

under the trade names of Estane®, Texin® and Pellethane®, respectively [3]. The structure–property relationships of segmented TPUs have been extensively studied by Tobolsky and Cooper [4–6], Bonart et al. [7–10] and Wilkes et al. [11–13]. It is interesting to note that evidence of a spherulitic superstructure in segmented thermoplastic urethane systems with well-defined monodisperse hard segment lengths was first presented by Samuels et al. [14] in 1971. In 1972, Dupont commercialized thermoplastic polyetheresters [3] derived from terephthalic acid, tetramethylene glycol and polytetramethylene oxide (PTMO) under the trade name Hytrel®. Since then, a large research effort has been directed towards understanding the influence of the chain structure and crystallization conditions on the morphology of these specific segmented materials. Various morphological models have been proposed by Cella [15], Seymour [16], and Wegner [17]. Wegner and his coworkers [18] also studied the crystallization of segmented polyetheresters under various conditions and observed that the type of supermolecular structure such as spherulites, formed from the organization of individual crystalline lamellae not surprisingly depends on the crystallization conditions in addition to chain structure.

In the late 1960s and early 1970s, various research groups also explored the possibility of synthesizing TPEs by covalently linking ether blocks to amide blocks via amide, urethane or urea linkages to give thermoplastic poly(ether-*block*-amide) [3]. However, it was not until the discovery of the tetraalkoxide catalyst family by Atochem that the synthesis of sufficiently high molecular weight poly(ether-*block*-amide) with ester linkages was made possible [19]. In the early 1980s, Atochem introduced thermoplastic poly(ether-*block*-amide), commercially known as PEBAX® [20]. These TPEs consist of linear chains of hard polyamide (PA) blocks covalently linked to soft polyether (PE) blocks via ester groups. The molecular weight of the PE blocks varies from about 400 to 3000 g/mol and that of the PA blocks varies from about 500 to 5000 g/mol. These poly(ether-*block*-amide) are synthesized via a metallic $Ti(OR)_4$ catalyst which facilitates the melt polycondensation of carboxylic acid terminated amide blocks with polyoxyalkylene glycols. The polymerization reaction is carried out at elevated temperatures (ca. 250 °C) and under high vacuum [3]. The general structural formula of these block copolymers is

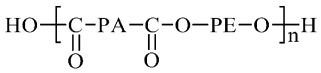

Due to the fact that these TPEs contain polyether blocks as well as polyamide blocks yet these two are interconnected by ester linkages, they have been often included in treatises on polyethers, polyamides or polyesters. Atochem uses nylon 12 and PTMO in its PEBAX XX33 series, where XX represents the shore D hardness of the material. Carboxylic acid termination of nylon 12 is promoted via reaction with adipic acid. Various nylons (such as nylon 6, nylon 11, nylon 12, etc.) have also been used as the PA block. Similarly, PTMO, polypropylene oxide (PPO) or polyethylene oxide (PEO) has been used as the PE block to synthesize thermoplastic poly(ether-*block*-amide) in other research laboratories [21–25]. Deleens et al. [26–29] have conducted a study of different precursors, catalysts and polymerization processes employed to synthesize these materials. Their mechanical properties such as stress–strain behavior, hysteresis, compression set, abrasion resistance, and tear strength have also been reported by Deleens [3]. Deleens notes that, 'The hysteresis values for PEBA are lower than those for thermoplastic or vulcanized materials of equivalent hardness'. Lacabanne and Faruque [30] used thermally stimulated current method while Xie and Chamberlin [31], Alberola [32], and Bornschegl et al. [33] used dynamic mechanical analysis (DMA) and differential scanning calorimetry (DSC), to study the thermal transition behavior of poly(ether-*block*-amide) materials. Nuclear magnetic resonance (NMR) and X-ray diffraction were also used by Hatfield et al. [34] to investigate the chain conformation in the crystal phase for poly(ether-*block*-amide) based on PEO and nylon 11 or nylon 12. They concluded that the PEO–nylon 11 or PEO–nylon 12 based poly(ether-*block*-amide) exist as microphase separated systems consisting of crystallites of PA surrounded by interfacial amorphous PA and PE phases. Furthermore, below ca. 0 °C the PE phase can also crystallize. Yu et al. [21–23] used small angle X-ray scattering (SAXS) to investigate the morphology of PPO–nylon 6 based poly(ether-*block*-amide) consisting of varying lengths of the two types of segments as well as their content. They also concluded that the PPO–nylon 6 systems are microphase separated. When the block lengths are relatively short, thereby restricting the development of folded chain lamellae, the PA phase was speculated to form more of a fringed micelle semicrystalline texture in an amorphous phase of PPO. The poly(ether-*block*-amide) systems with the longest block lengths investigated did, however, exhibit chain-folded crystals of the hard phase with enhanced interconnectivity of the hard phase as well as continuity of the soft phase. Strain-induced crystallization of the PTMO soft segment and its melting behavior in PEBAX 2533 and 3533 were investigated by Warner [35] (a topic that will also be addressed in this paper). Niesten et al. [36,37] compared a poly(ether-*block*-amide) consisting of aramid units of uniform length as the hard block and PTMO as the soft block with a commercial polyetherester (Arnitel® by DSM) and a commercial polyetherurethane (Desmopan® by Bayer). They found that the poly(ether-*block*-amide) could be used over a wider temperature range in comparison to comparable grades of Arnitel and Desmopan because of a low and sharp glass transition temperature, a temperature independent rubbery plateau, and a high and sharp melting transition. The ability of the aramid unit to crystallize faster and the higher heat stability of the poly(ether-*block*-amide)

are also favorable features of these materials during processing. More recently, Sauer et al. [38–40] used SAXS and atomic force microscopy (AFM) to specifically study the behavior of the crystalline phase in solution cast PEBAX 3533 under deformation.

There is little information, however, in the literature about the morphology of the entire nylon 12–PTMO based PEBAX XX33 series or any systematic correlation between the segment composition and morphological solid state structure of these materials and their resulting properties. The effect of sample preparation history has also not been investigated in detail. Thus the goal of this report is to address the structure of the PEBAX series (P2533, P3533, P4033, P6333, and P7033) via the techniques of DSC, DMA, AFM, SAXS, WAXS, small angle light scattering (SALS) and mechanical testing. An attempt has also been made to estimate the composition of the hard and soft segment contents of these materials by using solution NMR. Properties of these materials are thus explained on the basis of their segment composition, molecular structure and thermal and melt history although limited studies of films cast from solution were also undertaken. Furthermore, we have also attempted to study the effect of crystallization conditions on the morphology of thermoplastic poly(ether-*block*-amide).

2. Experimental materials and methods

2.1. Materials

Atofina Chemicals kindly supplied UV stabilized grades of PEBAX 2533, 3533, 4033, and 6333 in granular form. Unmodified PEBAX 7033, in granular form, was procured from Cordis Corporation. All resins were stored under vacuum at ambient until used.

2.2. Methods

Tensile testing was conducted via an Instron model 4400R equipped with a 1 kN tension load cell and calibrated with a 2 kg standard (19.61 N). The tensile tests were conducted at ambient temperature. 'Dog-bone' shaped specimens, 2.9 mm wide × ca. 0.33 mm thick, stamped out from compression molded films were used to generate the stress–strain curves at an initial strain rate of 1.5 mm/mm/min. A grip separation distance of 10 mm was used and a gauge length of 6 mm was assumed in order to calculate the elastic modulus and the percent elongation. Stress relaxation studies were performed on dog-bone shaped specimens 8.75 mm wide × ca. 0.4 mm thick using a grip separation distance of 25.4 mm. Percent elongation measurements were based on the grip separation distance and the samples were stretched at an initial strain rate of 40 mm/mm/min; the maximum allowed by the instrument.

DSC measurements were performed on a model SSC5200 Seiko Instruments DSC. All samples were heated from ambient temperature to 200 °C in order to erase any prior processing history of the samples. The temperature was then lowered to − 130 °C to collect DSC cooling data. A second heating scan produced the DSC heating profile. Both heating and cooling temperature scans were carried out at the rate of 20 °C/min under a dry nitrogen atmosphere.

A Seiko Instruments model DMS210 was used for the DMA measurements. The samples were heated under a dry nitrogen atmosphere from − 150 to 180 °C/min at the rate of 2 °C/min; tan δ and storage modulus, E', data were obtained at a frequency of 1 Hz.

SALS patterns of the deformed and the undeformed film samples were collected by using a HeNe linearly polarized laser with a wavelength of 632.8 nm. The polarization direction of the incident beam was vertical while the analyzer was horizontally oriented. This enabled the collection of the SALS data in the H_v mode [41]. A manual film stretcher was utilized to deform the samples which were 0.12 mm (4.7 mils) thick in their unstretched state. The SALS patterns were recorded by using an open back film camera; a sample to film distance of 34 cm was maintained throughout.

WAXS patterns were recorded via a Phillips X-ray generator; model PW1720, which produced nickel filtered Cu K_α radiation with a wavelength of 1.542 Å. The generator was operated at 40 kV and 20 mA. A Warhus camera with a pinhole collimation diameter of 0.020 in. was used to collect the patterns on a direct exposure imaging film. A sample to film distance of 5.0 cm was maintained throughout. Unstretched films with a thickness of ca. 0.45 mm were exposed for 2 h whereas the films stretched to 500% [6 ×] required an exposure time of 6 h due to the reduced sample thickness.

A Phillips X-ray generator, model PW1729, operating at 40 kV and 20 mA and generating nickel filtered Cu K_α radiation with a wavelength of 1.542 Å was used to record the SAXS profiles. The scattering patterns were collected by a Kratky camera with a 0.03×5 mm^2 slit collimation in conjunction with a Braun OED50 position-sensitive detector. A film thickness of ca. 0.42 mm was used for all the samples. The raw scattering data was corrected for parasitic scattering and normalized by sample thickness and exposure time. The intensity data was also normalized by using a Lupolen standard.

Films utilized for SALS, WAXS, and SAXS were melt compression molded at ca. 200 °C and were slow cooled in air.

Tapping mode AFM was utilized to study the morphology of the PEBAX samples. Free surfaces of solution cast and melt compression molded films were studied via a Digital Instruments Dimension 3000 scanning probe microscope (controlled by a Nanoscope IIIa controller) which used Nanosensors' tapping etched silicon probe type single beam cantilever tips. The cantilevers, with a length of ca. 125 μm and force constants of 35 ± 7 N/m were used at

oscillation frequencies of ca. 290 kHz. 3 and 1 μm images were taken by maintaining a set point ratio (ratio of the magnitude of the engaged amplitude to the free air amplitude of the oscillating silicon tip) of ca. 0.6.

The compositions of the PEBAX samples were determined via ^{1}H NMR. A Varian Unity 400 spectrometer at 400 MHz was used to perform the ^{1}H NMR analysis in deuterated trifluoroacetic acid at ambient temperature. The chemical shifts were referenced to three peaks that were not convoluted with other peaks in the ^{1}H NMR spectra and the compositions were reported as the average of these three peaks. These reference peaks were the methylene peaks next to the oxygen on PTMO at ca. 3.9 ppm, next to the nitrogen of nylon 12 at ca. 3.6 ppm, and next to the carboxyl of the adipic acid at 2.6 ppm, respectively. The results of the analysis have been presented in Table 1.

3. Results and discussion

3.1. Mechanical properties

3.1.1. Dynamic mechanical analysis

DMA results for the series of PEBAX materials are shown in Fig. 1(a) and (b) which provide the data for E' and tan δ, respectively. In Fig. 1(a), one notes that, in general, the storage modulus behavior tends to display four particular regions although there are some additional subtleties. In brief, at low temperatures in the range of -150 to -100 °C, all materials are glassy but beginning at about -100 °C, those systems with the highest PE content undergo a softening which arises from the glass transition behavior of the PE segment. That transition, as expected, is not particularly distinct for the highest two PA containing materials (P6333 and P7033). Following this transition, there is then a general 'rubbery' plateau behavior in the modulus that extends from the order of 0 to 150 °C whose extensions to higher temperature is greater for higher PA containing materials. This general plateau region of course is more of the 'service window' for many of the applications these materials would be utilized for since there is a relatively low dependence of

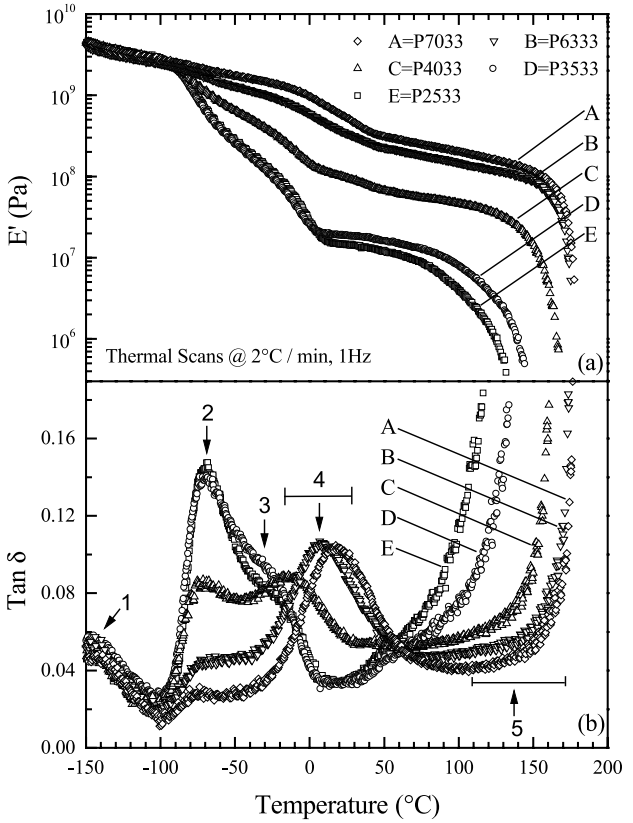

Fig. 1. DMA scans of slowly cooled melt compression molded PEBAX films. (a) Storage modulus. (b) tan δ. Note: transitions have been numbered 1–5, with transitions #4 and #5 indicated by a general temperature range.

stiffness on temperature. Above the rubbery plateau region, a decline in E' occurs that extends from the melting characteristics of the PA segment. This onset of E' decline systematically occurs at lower temperatures as the T_m decreases (lower PA content). Further support of this latter point will also be provided in the later discussion of the DSC analysis.

Possibly more revealing with respect to the thermal transition response as noted by DMA extends from the corresponding tan δ data shown in Fig. 1(b). It may be noted that the transitions have been labeled as #'s 1–5 accordingly with both #4 and #5 being indicated by a general range of

Table 1
Composition of PEBAX samples as determined via ^{1}H NMR

Sample	Composition (mol%)					
	PTMO		Nylon 12		Adipic acid	
	Present work	Ref. [42]	Present work	Ref. [42]	Present work	Ref. [42]
P2533	84.68 ± 0.07	87.1	11.92 ± 0.06	8.0	3.40 ± 0.01	4.9
P3533	83.61 ± 0.07	74.9	13.00 ± 0.03	21.2	3.39 ± 0.04	3.9
P4033	70.41 ± 0.01	74.0	27.15 ± 0.04	22.8	2.44 ± 0.02	5.5
P6333	36.96 ± 0.02	–	60.47 ± 0.04	–	2.57 ± 0.04	–
P7033	24.78 ± 0.05	–	72.95 ± 0.01	–	2.27 ± 0.04	–

Note: as received P2533, P3533, P4033, and P6333 resins (supplied by Atofina Chemicals) contained UV stabilizers.

transition temperatures as will be explained shortly. Beginning from low temperatures, the transition labeled #1 is really a convolution of separate transitions that occur in the respective amorphous PA and PE phases since both homopolymeric nylon 12 and PTMO display small transitions in these same regions that arise from local motion of methylene sequences that exist in each polymer [43,44]. Turning attention to transition #2, this distinctly arises from the PTMO glass transition as confirmed by many examples in the literature, which have observed such a behavior in segmented polymers that contain PTMO as a soft segment [3,25,33]. Of note is the fact that the magnitude of transition #2 in the range of $-70\,^{\circ}C$, as would be expected is consistent with the PE content of the respective samples. Particularly noteworthy are the nearly equal magnitudes of transition #2 in P2533 and P3533, respectively, which is consistent with their nearly equal PTMO contents (recall Table 1). The dependence of the magnitude of transition #2 on the PE content of the sample provides support for the microphase separation behavior of this component. Furthermore, the T_g of the PE phase appears relatively independent of the PE content of the sample and occurs at a higher temperature than the homopolymeric PTMO T_g (reported to be at $-75\,^{\circ}C$ via DMA [44]). Such a behavior alludes to the presence of a PE amorphous phase consisting largely of PTMO segments mixed, at best, with only a small amount of nylon 12 segments. What stands out is the fact that the upper side of transition #2 influences the magnitude of transition #3 which arises from the partial cold crystallization and melting behavior of the PTMO phase where melting is completed in the range of $0\,^{\circ}C$. Further strong support for this interpretation will be provided later from our DSC analysis. However, in the range of transition #3 and extending upward into the region designated as #4, the damping again increases due to the glass transition characteristics of the PA component. As is noted for samples P4033, P6333 and P7033, the peak designated as transition #4 is particularly distinct and moves to higher temperatures as the overall PA content of the sample increases. The other two PA containing segmented materials do not display a significant PA T_g response. Such behavior is due to the fact that the PA segments are shorter and possibly further mixed with some of the PE material, giving rise to a broadening and a downward shift in its T_g. Thus transition #4 becomes convoluted into the region where the PE crystal soft segments melt is associated with transition #3. The general characteristics of the PA glass transition temperature can be discerned again by inspecting the three higher PA containing compositions when noting the respective E' data in Fig. 1(a). Finally, with regard to transition #5, which has been addressed when discussing Fig. 1(a), the rise in tan δ is simply due to the onset of the melting characteristics of the PA crystal phase. Again, further support for this interpretation will extend from the DSC behavior that will be presented in Section 3.2.

3.1.2. Tensile deformation behavior

The stress versus strain response exhibited by the PEBAX series, shown in Fig. 2, is consistent with their segment composition. Samples P2533 and P3533, with relatively low hard PA segment content, behave as elastomers; they exhibit a low Young's modulus and a remarkably high elongation at break. The lack of a distinct yield point in these samples provides further support to the above observation. It may be noted that in the case of P2533 and P3533 the strain at break exceeds 1000% even when the calculation of the strain values is based on the grip separation distance (10 mm) instead of the gauge length (6 mm) and any slippage of the samples from the grips at high strains is taken in to account. On the other hand, a sharp yield point can be observed in both P6333 and P7033. They exhibit a higher Young's modulus and their elongation at break is considerably lower. Such a behavior suggests an increase in the hard phase connectivity of the PEBAX materials with increasing PA content. Thus P6333 and P7033 act more like hard thermoplastics than elastomers. Furthermore, as a result of the increase in the interconnectivity of the hard phase, there is a systematic increase in the Young's modulus (see tabulated values in Fig. 2) of the PEBAX series with PA content.

The energy of rupture normalized per unit volume of the initial sample, calculated by integrating the stress–strain curve, is higher for P3533 (399 MJ/m^3) as compared to P2533 (296 MJ/m^3). This follows from the fact that P3533 has a comparable value of elongation at break in spite of sustaining a higher load at any given strain. However, the energy of rupture per unit volume systematically decreases for samples with higher PA content; from 208 MJ/m^3 in P4033 to 206 and 113 MJ/m^3 in P6333 and P7033, respectively. The area under the stress–strain curve is also a measure of the toughness of the material. Thus under these test conditions, P3533 is the toughest material within the

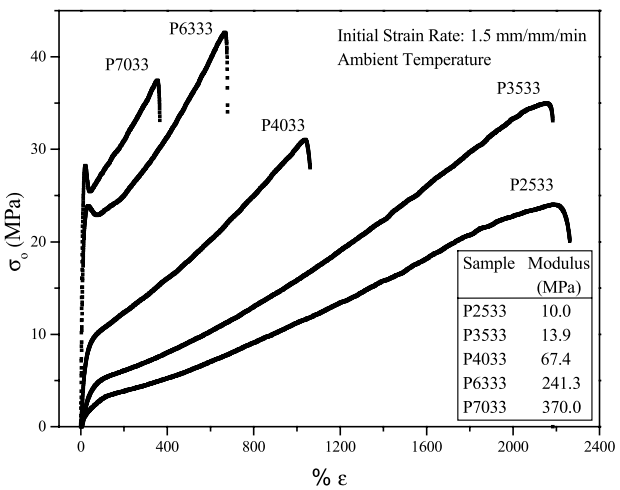

Fig. 2. Stress versus strain behavior of slowly cooled melt compression molded PEBAX films. Note: Young's modulus values of the samples have been tabulated in the inset.

series and materials with higher PA content exhibit a systematic decrease in toughness.

3.2. Thermal analysis

The cooling and the second heating thermal scans are shown in Fig. 3(a) and (b), respectively. In the cooling scan, the PEBAX samples with lower PA content show two crystallization peaks, ΔH_c, one for the PA segments at the higher temperature and the other due to the crystallization of the PE segments at the lower temperature. The amount of relative crystallinity due to the PE phase, as reflected by ΔH_c, is the highest in P2533 and it decreases with decreasing PE content of a sample until it cannot be observed in P6333 and P7033. Conversely, the amount of crystallinity due to the PA phase increases with increasing PA content. At the same time, the onset of crystallization shifts to higher temperatures and hence to earlier times in the cooling cycle with increasing PA content (there being one exception to such a trend, namely P7033). However, there is no significant change in the crystallization temperature of the PE blocks for the three samples (P2533, P3533 and P4033) that show PE crystallization across the series.

The second heating scans show the melting of these crystalline phases; the PE melting peak (in the range of 7–10 °C) decreases in intensity until it cannot be observed in P6333 and the PA melting peak increases with increasing PA content of the sample. Most of the PE crystals have completely melted in the high PE content materials, such as P2533 and P3533 by the time the material reaches room temperature. It might be noted that all the peak T_m values of the PE segments for the undeformed samples were distinctly lower than those reported for homogeneous PTMO, i.e. 35–43 °C [44,45]. This lower peak T_m behavior of the PE segments undoubtedly arises from their inability to develop thicker more perfect lamellae crystals that can be promoted in the respective homopolymer—in fact for the low PE containing systems, folded chain PE lamellae would seem to be difficult to form in view of many short segment lengths [21–23]. In contrast to the nearly constant peak melting point, at ca. 7 °C, of the PE phase, the PA melting point systematically increases with increasing PA content as does the associated magnitude of the respective value of ΔH_f. Yu et al. [21–23] reported that compression molded films of PPO–nylon 6 poly(ether-*block*-amide) having relatively short soft segments exhibited multiple PA endotherms. The melting of lamellae of different thickness was offered as a possible explanation for such an observation. We did not observe multiple PA endotherms but the shifting of the PA melting point to higher temperatures is very distinct and could be due to an increase in the perfection of the PA crystalline phase and/or increased lamellar thickness (both of which may occur due to a systematic increase in the PA block length with PA content). In contrast to the DMA data, the glass transition temperature of the PE phase is difficult to discern from the DSC thermal scans due to broad transitional behavior but it is well below −50 °C. It may be recalled that a relatively composition invariant PE phase T_g at ca. −70 °C was observed via DMA. The T_g of homopolymeric PTMO as determined via DSC has been reported to be −82 °C [25].

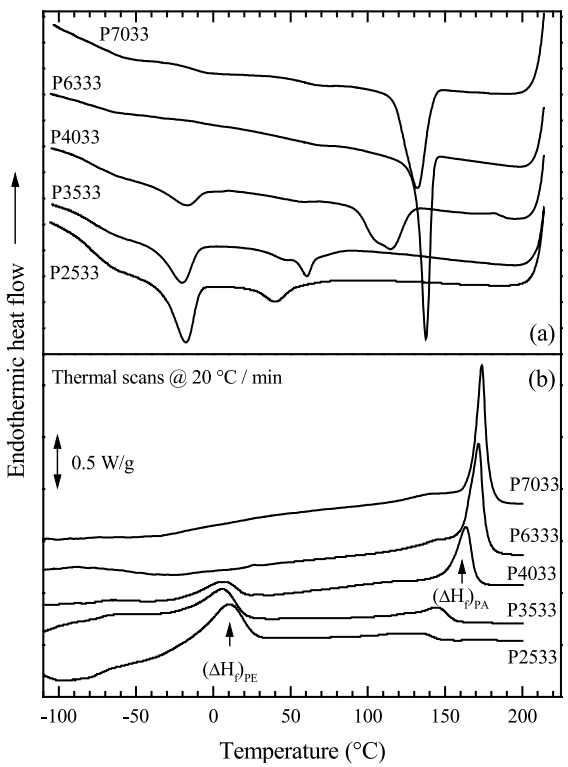

Fig. 3. DSC scans of slowly cooled melt compression molded PEBAX films. (a) Cooling thermal scans; (b) second heat thermal scans. Note: traces have been displaced vertically for clarity.

3.3. Wide angle X-ray scattering

The wide angle X-ray scattering (WAXS) patterns at ambient conditions for the undeformed and the uniaxially stretched (to 500%) PEBAX samples are shown in Figs. 4 and 5, respectively. The amorphous halo principally due to the PE phase, distinctly seen in the undeformed P2533 sample, gradually fades as the PE content decreases. On the other hand, the Bragg reflections due to the PA crystalline phase become sharper with increasing PA content of the samples. In the undeformed state, the unit cell of the nylon 12 crystals have been reported to be monoclinic [46]. Since the PEBAX samples utilized for the WAXS study were not cooled below room temperature, no reflections that can be attributed to the PE phase are expected to be seen in the undeformed samples. It may be recalled that the DSC cooling scans (Fig. 3(a)) showed that the cold crystallization of the PE blocks does not begin until about 0 °C.

All the PEBAX samples when stretched (at ambient) to 500% clearly show two reflections on the meridian that can be attributed to the PA crystal phase. These spots systematically darken with increasing PA content. Norholt et al.

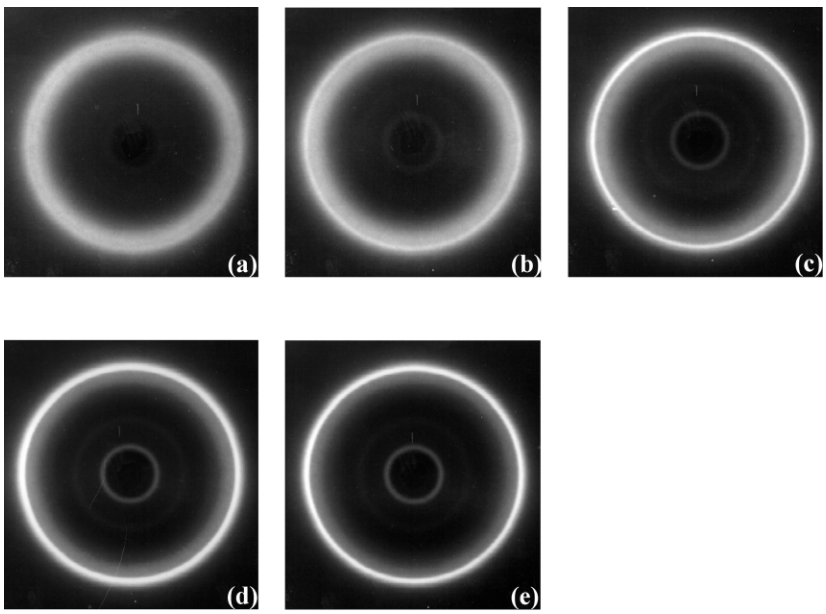

Fig. 4. WAXS patterns of undeformed slow cooled melt compression molded PEBAX films. (a) P2533. (b) P3533. (c) P4033. (d) P6333. (e) P7033.

[47] while studying polymorphism in pure nylon 12 arising due to deformation also observed another reflection on the equator. This equatorial reflection, clearly seen in P4033, P6333 and P7033 cannot be easily distinguished in P2533 and P3533 because the PE phase, which is the major component in these two systems, undergoes strain-induced crystallization and the two resulting PE phase equatorial reflections overlap the equatorial reflection of the PA crystal phase. However, as the PE content decreases, the situation reverses itself and in P7033, which has the highest PA content within the series, only a single equatorial reflection due to the PA crystal phase is seen.

Using both materials of P2533 and P3533, Warner [35] found that a strain of ca. 500% was required before the PE phase underwent strain-induced crystallization at ambient temperature. Upon stretching these same materials to 700% we also found the expected PE crystal phase equatorial reflections in the WAXS patterns as shown in Fig. 6(a). We also allowed the stretched samples to *freely relax* and later subjected them to a heating scan in the DSC beginning from the ambient. The melting of the PE crystal phase can be clearly seen from the DSC data shown in Fig. 6(b). Furthermore, and as expected, the amount of crystallinity (determined by ΔH_f) due to the strain-induced crystalline PE phase is higher in P2533 than in P3533.

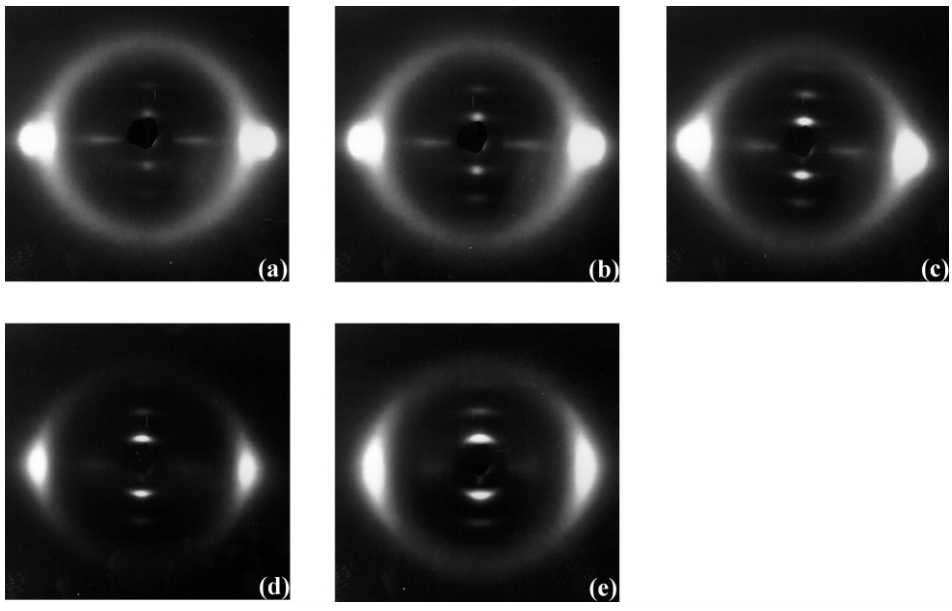

Fig. 5. WAXS patterns of slow cooled melt compression molded PEBAX films uniaxially stretched to 500%. (a) P2533. (b) P3533. (c) P4033. (d) P6333. (e) P7033. Note: stretch direction is vertical.

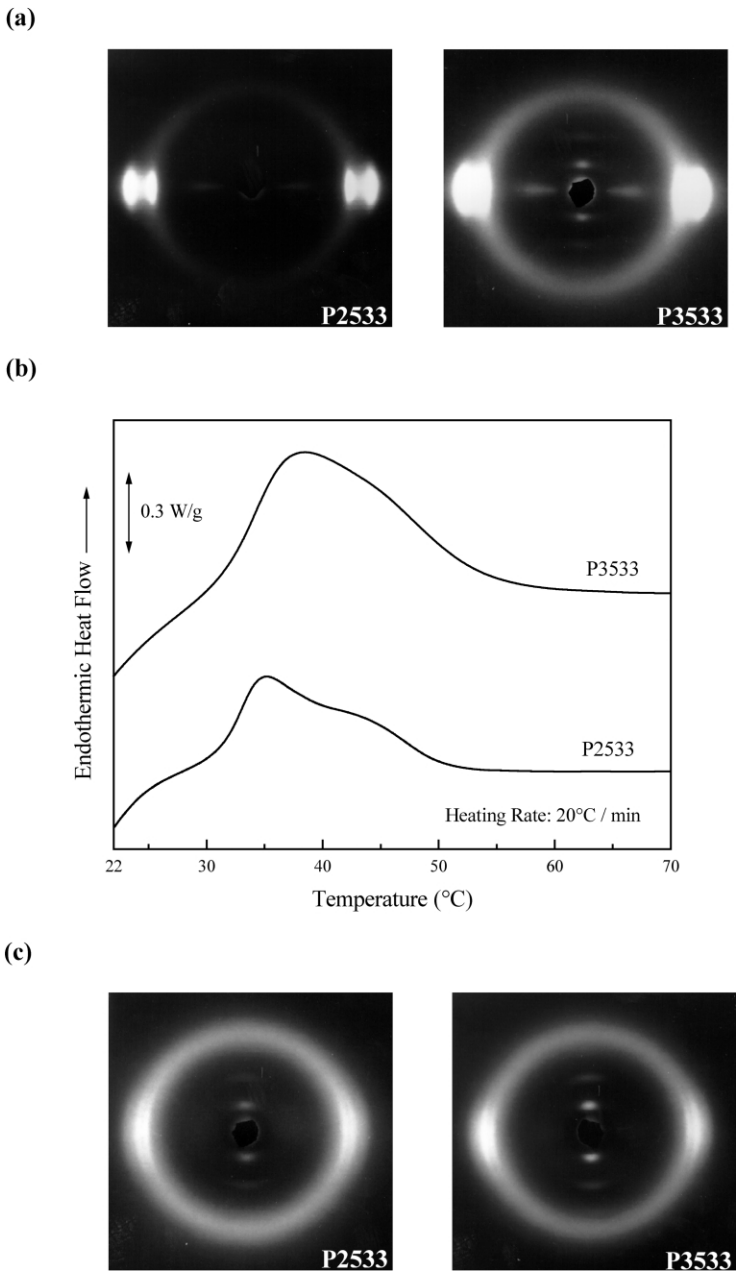

Fig. 6. Strain-induced crystallization of slow cooled melt compression molded P2533 and P3533. (a) WAXS images of samples stretched to a draw ratio of 8 ×. (b) DSC thermal scans of freely relaxed samples. Traces have been displaced vertically for clarity. (c) WAXS images of freely relaxed samples annealed at 70 °C for 90 min. Annealed samples P2533 and P3533 exhibited a permanent set of 63 and 97%, respectively, when measurements were made immediately after the annealed samples cooled down to room temperature. Note: stretch direction in WAXS patterns is vertical.

Of note is the similarity in the strain-induced crystallization and general melting range behavior of the PE segments in samples P2533 and P3533 to that of the well-known strain-induced crystallization characteristics of very lightly cross-linked natural rubber. Specifically, this latter material, when stretched sufficiently, can be promoted to develop a high enough crystalline content to induce inelastic behavior (high permanent set) which arises from a row nucleated crystalline phase [48]. Upon heating such an inelastic material, the crystals melt in the range of ca. 30 °C and elasticity is again restored, as it also is when the strain-induced crystals of the PE phase are melted as well. While the PE strain-induced crystalline amount is undoubtedly lower than that promoted in highly stretched (racked) [49] natural rubber, these PE crystals, in conjunction with those already present in the crystalline PA phase, provide sufficient rigidity such that inelastic behavior (high permanent set also) occurs. Again, when the PE crystals are melted, elasticity is restored. The result of this similarity in strain-induced crystallization and melting behavior has promoted the samples P2533 and P3533 to be considered for heat shrink materials, as has been the case for racked natural rubber [35,50–53].

Inelastic samples of P2533 and P3533 (due to strain-induced crystallization upon stretching to 700%) were allowed to freely relax and then annealed at 70 °C for 90 min and slowly cooled in air to ambient temperature. It may be noted that the annealed samples exhibited a permanent set of 63 and 97%, respectively, when measurements were made immediately after the annealed samples cooled down to room temperature. The WAXS patterns of these samples, shown in Fig. 6(c), show a darkening of the amorphous halo as compared to the stretched and unannealed samples. As expected, the amorphous halo darkens while the equatorial reflections due to the PE crystal phase fade. Furthermore, the equatorial reflections due to the residual oriented PA crystal phase can also be seen and the PA reflections at the equator and at the meridian are darker in P3533 than in P2533.

3.4. Surface morphology via AFM

The free surfaces of PEBAX films prepared from the melt were imaged via tapping mode AFM at ambient temperature and the resulting phase images are shown in Fig. 7. A 'free' surface was obtained from a melt compression molded film by reheating the film to ca. 20 °C above the highest melting transition of the respective sample in a hot stage. The sample was maintained at this temperature for ca. 2 min and allowed to cool to ambient temperature at 30 °C/min. Under the tapping conditions used to image the samples, a high phase angle corresponds to high stiffness regions at the surface. In the particular case of the PEBAX series, at ambient temperature the PE phase is expected to behave as a soft rubbery phase and thus correspond to regions of low phase angles in the AFM phase images. The interpretation of the high phase angle regions, however, is more complicated. At ambient temperature, the amorphous PA domains behave as a glassy solid (Fig. 3). Thus when the AFM imaging of these samples is undertaken under ambient conditions the stiffer regions seen by the AFM tip could possibly correspond to either the amorphous (glassy) or the crystalline regions of the PA blocks. Due to this fact one cannot easily assign the stiffer regions seen in the tapping mode AFM phase images (of P6333 and P7033 taken at ambient temperature) exclusively to the crystalline PA regions. However, as seen from Fig. 7, the presence of a spherulitic morphology on the free surface of the melt pressed P6333 and P7033 films is clearly evident. Furthermore, for this crystallization condition a larger spherulite size in P7033 is indicated. As will be discussed later, the results obtained using SALS are in agreement with the AFM results. It may be noted that in the case of polyetherester based segmented TPEs various researchers [14,15,54,55] have shown the ability of the polyester hard blocks to crystallize and also give rise to a spherulitic superstructure. Melt compression molded samples of P2533 (not shown), P3533, and P4033 do not clearly indicate the presence of a spherulitic superstructure and our SALS data (to be presented later) provides further support to the AFM results. However, it may be recalled from the DSC results (Fig. 3) that P2533, P3533, and P4033 also have a PA crystal phase.

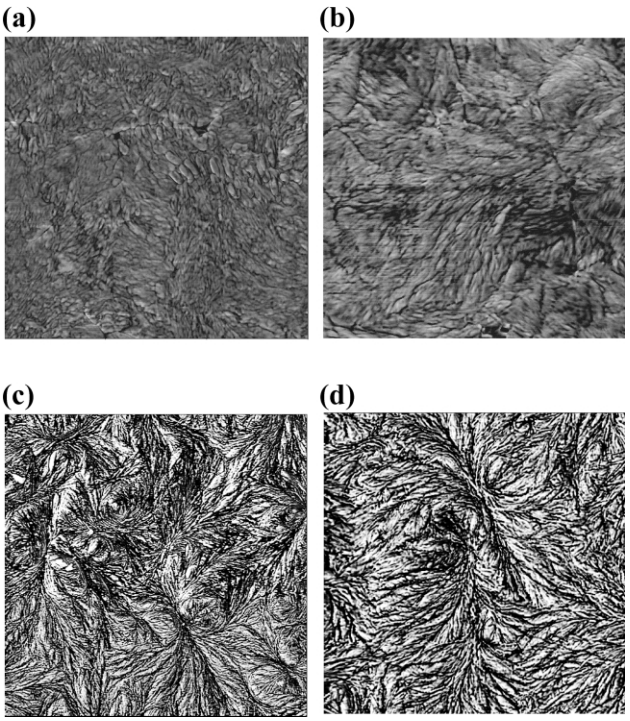

Fig. 7. Tapping mode AFM phase images of the free surface of melt compression molded PEBAX films. Images are at a magnification of 3 μm × 3 μm. (a) P3533, (b) P4033, (c) P6333, and (d) P7033.

A limited investigation of the surface morphology of PEBAX films cast from solution (5 wt% in dimethyl acetamide) was also undertaken via tapping mode AFM in order to compare the morphology of the free surfaces of melt versus solution cast films. The phase images of solution cast films of samples P3533, P4033 and P7033 taken at ambient temperature via tapping mode AFM are shown in Fig. 8(a)–(c). Sample P2533 was also investigated but we were unsuccessful in obtaining a useful phase image of this specific material. Recall that P2533 is highly dominated by the soft PTMO component. In our previous discussion it was noted that since the amorphous PA phase behaved as a glassy solid in the vicinity of the ambient temperature, it was difficult to distinguish the high phase angle regions seen in AFM phase images into crystalline PA and amorphous PA phases. The same problem is encountered in the present case; however, the presence of long and slender stiff PA regions can be clearly seen in the phase images of samples P3533 (Fig. 8(a)) and P4033 (Fig. 8(b)). From such an observation it may be inferred that when cast from moderately dilute solutions, the PA crystalline phase in P3533 and P4033 forms lamellar crystals that are rather randomly ordered. P4033 has evidently thicker lamellae than does P3533. Such a visual observation could result when the lamellae are not oriented perfectly normal to the

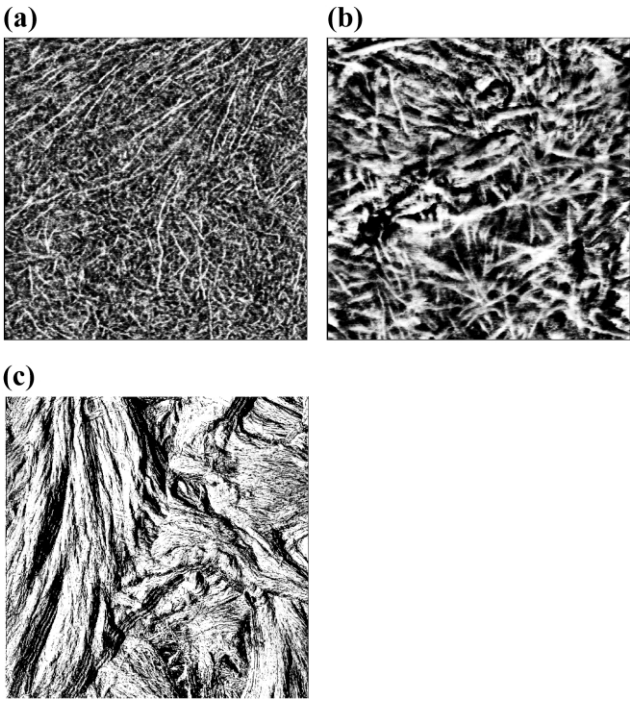

Fig. 8. Tapping mode AFM phase images of PEBAX film cast from 5 wt% DMAc solution. (a) 1 μm × 1 μm image of P3533. (b) 1 μm × 1 μm image of P4033. (c) 5 μm × 5 μm image of P7033.

free surface and thus does not necessarily suggest that the lamella thickness in solution cast PEBAX samples increases with the PA content of the sample. As mentioned earlier, the techniques of AFM (and 2D SAXS) were used by Sauer et al. [38–40] to study the deformation behavior of the crystalline PA phase in solution cast P3533 films. They also observed the presence of randomly oriented lamellar PA crystals in undeformed P3533 films. At strains above 1.5 ×, break-up of these lamellar crystals resulted in smaller crystals with lower aspect ratios accompanied by a progressive formation and orientation of load bearing nano-fibrillar crystals.

Turning attention to P7033, one notes that it has the highest PA content in PEBAX series investigated, which gives rise to a highly interconnected PA hard phase. The presence of such a high interconnectivity within the PA hard phase can be clearly seen in the AFM phase image of the free surface of the solution cast P7033 film (Fig. 8(c)). However, there is no indication of the formation of a spherulitic morphology as was seen on the free surface of the melt compression molded P7033 film (Fig. 7(b)).

3.5. Bulk morphology via SALS

Optically anisotropic spherulitic superstructure in a polymer film can generally be detected via SALS. AFM is a surface technique whereas SALS is bulk technique. Hence it was believed necessary to determine via SALS whether the spherulitic structure observed in P6333 and P7033 via tapping mode AFM was also present throughout the bulk of a given sample. SALS images of the slow cooled undeformed, deformed, relaxed and annealed samples were obtained and are shown in Fig. 9. Slow cooled melt compression molded films of P6333 (Fig. 9(a)) and P7033 (Fig. 9(b)) clearly show the presence of optically anisotropic spherulites. A fourfold symmetric cloverleaf pattern was, however, not seen in P2533, P3533 and P4033 suggesting the absence of a sufficiently well defined optically anisotropic superstructure in these samples. In fact no significant H_v light scattering intensity was noted for these three samples. Thus these results are in agreement with earlier AFM results of melt compression molded PEBAX films.

The average radius, R, of the spherulites can be determined from the H_v pattern [41] of the undeformed sample by the relationship

$$4.13 = \frac{4\pi R}{\lambda_m} \sin\left(\frac{\theta_{max}}{2}\right) \quad (1)$$

where λ_m is the wavelength of the incident beam (632.8 nm) divided by the average refractive index of the polymer and θ_{max} is the radial scattering angle defined by the maximum in the scattering intensity in any lobe of the H_v pattern. The refractive indices of slow cooled melt compression molded films P6333 and P7033, determined via a Metricon model 2010 prism coupler were 1.5137 and 1.5212, respectively. Based on the above equation, the average diameter of the spherulites in P6333 and P7033 was calculated to be 7.3 and 18.1 μm, respectively. On comparison of the average size of the spherulites in P6333 and P7033 as determined via SALS and AFM (Fig. 7) one notes that the AFM images indicate a smaller spherulite size (higher nucleation density). This is due to the fact that melt compression molded P6333 and P7033 films were cooled at a higher rate in the hot stage as compared to the rate of cooling that resulted when freely cooled in air outside the hot stage. It may be noted that the melt compression molded films of P6333 and P7033 that were quenched in ice water did not shown any indication of a four fold symmetric cloverleaf pattern suggesting the absence of a distinct optically anisotropic spherulitic superstructure in quenched samples.

The slow cooled and undeformed P7033 films were also uniaxially stretched up to 150% and SALS images were taken at 15 and 150% strain, respectively. At 15% strain, P7033 is within the linear region of the stress–strain curve (recall Fig. 2). Even at such a low deformation, as can be seen from Fig. 9(c), elongational and shear stresses are propagated through the PA crystal phase resulting in deformation of the spherulites. At 150% strain, P7033 has gone through the yield point (at ca. 25% strain) and is well within the nonlinear region of the stress–strain curve. Significant deformation of the spherulite occurs at such high strains (Fig. 9(d)). The stretched P7033 sample was then allowed to *freely relax* at ambient and it was subsequently annealed at 90 °C for 90 min and slowly cooled in air. P7033 freely relaxed to a strain of 102% and after annealing exhibited a permanent set of 70%. The SALS image of the

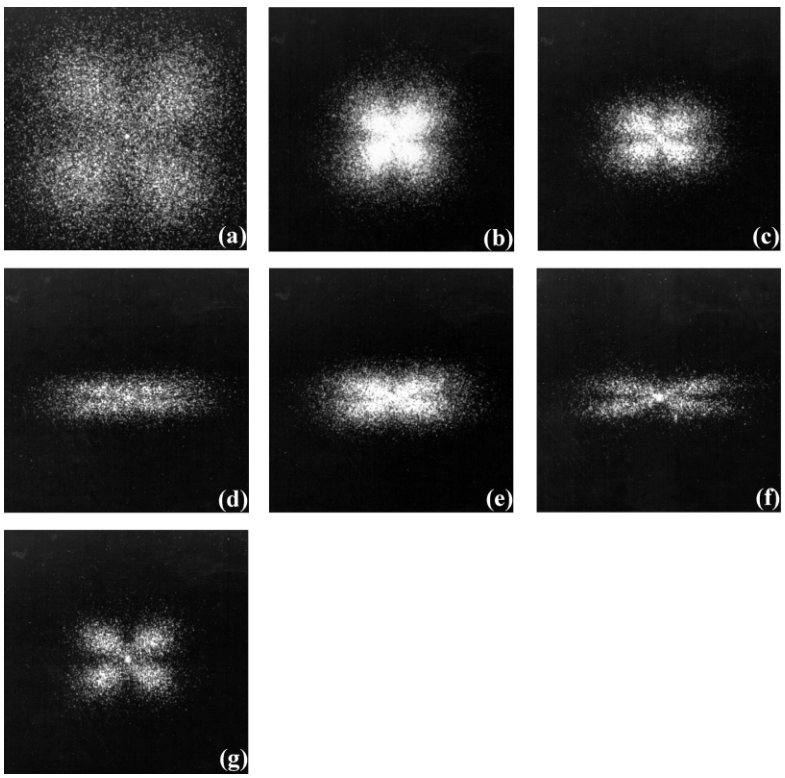

Fig. 9. H_v SALS patterns of slow cooled melt compression molded PEBAX films at a sample to film distance of 340 mm. (a) Unstretched P6333. (b) Unstretched P7033. (c) P7033 stretched to 15%. (d) P7033 stretched to 150%. (e) Stretched P7033 allowed to relax and annealed at 90 °C for 90 min. After annealing the sample relaxed to 70%. (f) P7033 stretched to 70%. (g) Stretched P7033 allowed to relax and annealed at 90 °C for 90 min. After annealing the sample relaxed to 31%. Note: stretch direction is vertical.

annealed sample is shown in Fig. 9(e). A melt compression molded film of P6333 was also subjected to a identical deformation experiment. After annealing, a permanent strain of 50% was exhibited by P6333. As expected, this indicates that the permanent set is a function of the PA content of the sample. For purposes of comparison, an undeformed P7033 film was stretched to 70% to match the value of the permanent set of the annealed sample. This sample was then allowed to freely relax and was thereupon annealed at 90 °C for 90 min and then slowly cooled in air. After annealing, a permanent strain (set) of 31% was exhibited by P7033. SALS images of the stretched and annealed samples are shown in Fig. 9(f) and (g), respectively. Upon comparison of corresponding SALS images (Fig. 9(c) and (g), Fig. 9(e) and (f)) one notes the inability of the spherulitic superstructure in P7033 to completely recover its original shape. P6333 deformed under identical conditions, however, only exhibited a permanent set of 11% and the recovery of the spherulitic superstructure in this sample was more complete than that in P7033 suggesting the expected dependence of permanent set in a given sample on its PA content.

3.6. Small angle X-ray scattering

Researchers have utilized SAXS as an important technique to supplement other structural characterization tools to confirm the presence of a phase separated morphology in block copolymers. Information such as the degree of phase separation, the size distribution and interdomain spacing (when a periodic structure exists) of the domains and the thickness of the interphase (for e.g. between the amorphous and the crystalline phases) have been reported by examining different regions of the scattering curve [21–23,56,57]. The PEBAX samples investigated in the current report, however, present a more complex morphology to examine via 1D SAXS due to the presence of a PA crystal phase surrounded by phase separated PA and PE amorphous regions. This increases the difficulty in assigning the origin of a first order interference peak to that of a interdomain spacing or a classical 'long spacing' associated with lamellar crystals. While slit smeared and single meridinal scan data is difficult to interpret, it must be noted that a full 2D SAXS pattern can allow a much more complete structural analysis [38–40]. The 1D SAXS profiles of undeformed slow cooled melt compression molded PEBAX films are shown in Fig. 10. One notes the presence of a broad first order interference peak in all samples where the slit smeared d spacing nonsystematically varies from ca. 158 to 146 Å as the PA content of the sample increases. However, as mentioned earlier the complex morphology of these samples makes it difficult to interpret the full origin of scattering profile of one sample relative to the next. Therefore, in light of the

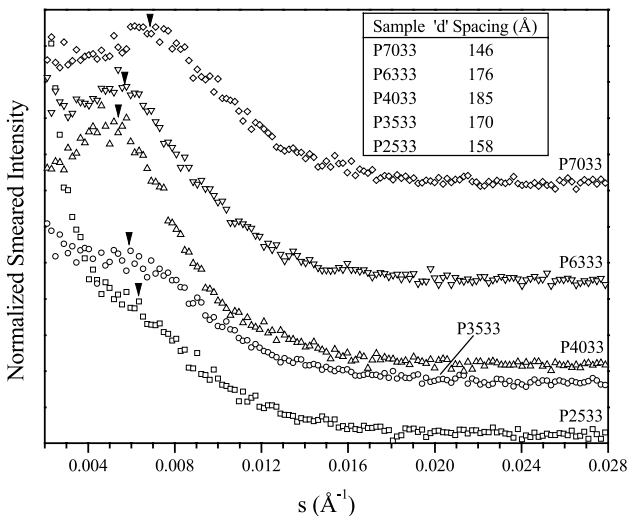

Fig. 10. SAXS profiles of slow cooled melt compression molded PEBAX films. (a) P2533. (b) P3533. (c) P4033. (d) P6333. (e) P7033. Note: *d* spacing of each sample has been tabulated in the figure inset.

multiphase complexity of the PEBAX materials, further analysis of the SAXS data did not seem warranted for this study.

3.7. Stress relaxation

Polymers typically exhibit a time dependent relaxation behavior when subjected to a constant deformation. Such phenomenon can be followed via stress relaxation. In many applications an elastomeric component may be subjected to an instantaneous fixed deformation and the component is expected to display a resisting force under these conditions for a fixed length of time. Thus it is of practical interest to investigate the relaxation behavior of the PEBAX samples. In view of the morphological picture of the PEBAX samples developed thus far one expects their stress relaxation behavior to be different when the deformation is within different regions of the respective stress–strain curves. Thus the stress relaxation measurements of the PEBAX samples were made at 7.5% strain (which is within the linear region of the stress–strain curve) and at 150% strain (which is well beyond the yield point of all the PEBAX samples investigated). The samples were deformed at an initial strain rate of 40 mm/mm/min and the tests were conducted at room temperature. Stress relaxation of a sample was quantified as the ratio of the absolute decrease in the stress at $t = 10\,000$ s to the stress immediately recorded after the sample was first stretched and the results are shown in Fig. 11.

At 7.5% strain (Fig. 11(a)), in samples with relatively high PE content (P2533, P3533, P4033) the relaxation occurs primarily in the activated PE phase, which has a higher degree of mobility at ambient temperature. Thus these samples exhibit a nearly linear stress relaxation behavior with log time. In samples P6333 and P7033 having

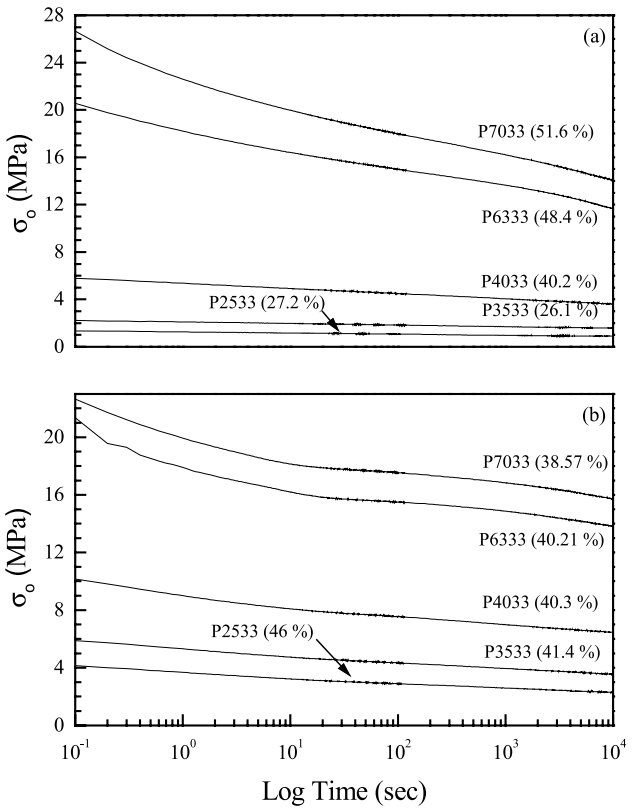

Fig. 11. Stress relaxation curves of slow cooled melt compression molded PEBAX films. Numbers in brackets indicate the ratio of the absolute decrease in stress at $t = 10\,000$ s to the stress immediately recorded after the sample was first stretched (a) at 7.5% strain, (b) at 150% strain.

a lower PE content, however, the stress relaxation behavior deviates markedly from linearity. This suggests that as the PE content of the sample decreases even the PA phase experiences the applied deformation and therefore the local PE phase deformation is strongly dependent on the PA content of the sample. The relaxation of the activated PE phase coupled with a significant relaxation of the deformed PA phase thus results in a nonlinear stress relaxation behavior in P6333 and P7033. Furthermore, the difference in the stress relaxation between P2533 and P3533 is statistically insignificant and it may be concluded that the degree of stress relaxation exhibited by a sample at small deformation increases with PA content.

At 150% strain (Fig. 11(b)), one notes that the percent stress relaxation values of the PEBAX samples are more or less independent of the PA content of the sample. This somewhat surprising behavior may be accounted by the fact that at a sufficiently high strain the PA hard phase experiences a significant degree of deformation and results in the break up of this partially interconnected rigid phase. The reader may recall the deformation of melt compression molded P6333 and P7033 films studied via SALS (Fig. 9) where a strain of 150% resulted in a significant deformation of the four leaf clover pattern indicating the considerable deformation experienced by the PA hard phase. Thus the local PE phase deformation is nearly independent of the PE

content of the sample and solely a function of the applied deformation. Consequently we see that the overall 'normalized' stress relaxation of a sample is nearly independent of the PA content of the sample.

4. Conclusions

Investigation of the solid state structure–property behavior of a series of nylon 12–PTMO based PEBAX thermoplastic elastomers with a systematic change in their PA content revealed a complex morphology that was strongly influenced not only by the PA content of a given sample but also by the sample's thermal and process history (melt versus solution). These multi block copolymers were found to be microphase separated with a relatively wide service temperature range of ca. 120 °C; between 0 and 120 °C for the relatively soft samples and between 30 and 150 °C for the relatively hard (higher PA content) samples. Both the constituent soft and hard segments were found to be crystallizable but the crystalline phase due to the soft PE segments completed the associated melting transition well below room temperature. The peak T_m of the PE crystalline phase was found to be lower than that reported for homopolymeric PTMO thus indicating the inability of the PE crystals to form well defined folded chain lamellae in these materials. The amount of crystallinity in a given sample, as determined via DSC, was found to increase with increasing PA content. On the other hand, DMA studies indicated the presence of mixed amorphous PE and PA phases. The PE amorphous phase contained a small amount of PA segments whereas the PA amorphous phase became richer in PA content as the overall PA content of the sample increased. The interconnectivity of the hard phase also increased with PA content and this resulted in a distinct yield point in the stress–strain response of compression molded P6333 and P7033, the two samples with the highest PA content within the series investigated. The Young's modulus and the extension at break exhibited a similar trend and a remarkably high extension at break was seen in the relatively soft samples P2533 and P3533. SALS and tapping mode AFM revealed the presence of a spherulitic superstructure in the bulk and on the surface, respectively, in compression molded samples P6333 and P7033. However, this form of morphological texture was diminished in samples with higher content of the PE soft segment. The spherulitic superstructure was found to deform at strains as low as 15% and this resulted in an incomplete recovery of the original sample dimensions upon release of the applied deformation. Deformation studies of P2533 and P3533 via WAXS revealed the ability of the soft PE segments to undergo strain-induced crystallization above 500% strain. Partial recovery of these samples resulted upon annealing above the melting temperature of the PE crystalline phase. The WAXS patterns also revealed the presence of a residual PA crystalline phase orientation in these samples. Stress relaxation behavior of compression molded samples at low strain was found to be dependent upon the PA content of a given sample, however, at high strain (beyond the sample yield point) it was found to be independent of the sample PA content. As expected, the soft P2533 and P3533 exhibited a linear stress decay with log time, which is often typical of many elastomeric materials. Tapping mode AFM of solution cast P3533 and P4033 revealed the presence of a lamellar PA hard phase randomly oriented in a matrix of the soft PE phase. A higher degree of PA interconnectivity was seen in solution cast P7033.

In summary, we conclude that the PEBAX samples exist as microphase separated materials at room temperature consisting of a PA crystalline phase in an amorphous matrix consisting of PE and PA segments. The morphology of both the crystalline and the amorphous phase appears to be dependent upon the PA content of the sample. Such a morphological model is consistent with other studies of poly(ether-*block*-amide) based on different soft and/or hard segments conducted by other research groups.

Acknowledgment

The authors gratefully acknowledge Mr. J. Lizotte and Prof. T.E. Long of the Dept. of Chemistry at Virginia Polytechnic Institute & State University for conducting the PEBAX composition analysis via ^{1}H NMR.

References

[1] Scollenberger CS (to Goodrich BF). US Patent 2,871,218; 1955.
[2] Scollenberger CS, Scott H, Moore GR. Rubber Chem Technol 1962; 35:742.
[3] Legge NR, Holden G, Schroeder HE, editors. Thermoplastic elastomers: a comprehensive review, 1st ed. New York: Hanser Publishers; 1987. Chapters 8 and 9.
[4] Cooper SL, Tobolsky AV. Tex Res J 1966;36(9):800.
[5] Cooper SL, Tobolsky AV. J Appl Polym Sci 1966;10(12):1837–44.
[6] Cooper SL, Tobolsky AV. Polym Prepr, ACS, Div Polym Chem 1967; 8(1):52.
[7] Bonart R. J Macromol Sci 1968;B2:115.
[8] Bonart R, Morbitzer L, Hentze GJ. Macromol Sci 1969;B3:337.
[9] Bonart R, Morbitzer L, Müller EH. Macromol Sci 1974;B9:447.
[10] Bonart R. Angew Makromol Chem 1977;58/59:259.
[11] Wilkes GL, Samuels SL. J Polym Sci 1973;43:149.
[12] Wilkes GL, Samuels SL. J Polym Sci, Polym Phys Ed 1973;11(4): 807.
[13] Wilkes GL, Bagrodia S, Humphries W, Wildnauer R. J Polym Sci, Polym Lett Ed 1975;13(6):321.
[14] Samuels SL, Wilkes GL. Polym Lett 1971;9:761.
[15] Cella RJ. J Polym Sci, Polym Symp 1973;42:727.
[16] Seymour RW, Overton JR, Corley LS. Macromolecules 1975;8:331.
[17] Wegner G, Fujii T, Meyer W, Lieser G. Angew Makromol Chem 1978;74:293.
[18] Zhu L-L, Wegner G. Makromol Chem 1981;182:3625.
[19] Deleens G, Foy P, Marechal E. Eur Polym J 1977;13:337.
[20] Deleens G. ANTEC 1981;419.
[21] Yu YC, Jo WH. J Appl Polym Sci 1994;54:585.

[22] Yu YC, Jo WH. J Appl Polym Sci 1995;56:895.
[23] Yu YC, Jo WH, Lee MS. J Appl Polym Sci 1997;64:2155.
[24] Bouma K, Wester GA, Gaymans RJ. J Appl Polym Sci 2001;80:1173.
[25] Boulares A, Tessier M, Maréchal E. Polymer 2000;41:3561.
[26] Deleens G, Foy P. French Patent 2,382,060; 1975.
[27] Deleens G, Guerin B, Poulain C. French Patent 2,359,879; 1976.
[28] Deleens G, Guerin B, Poulain C. French Patent 2,378,058; 1976.
[29] Deleens G, Ferlampin J, Gonnet M. French Patent 2,401,947; 1977.
[30] Faruque HS, Lacabanne C. Polymer 1986;27:527.
[31] Xie M, Chamberlin Y. Makromol Chem 1986;187:383.
[32] Alberola N. J Appl Polym Sci 1988;36:787.
[33] Bornschegl E, Goldbach G, Meyer K. Prog Colloid Polym Sci 1985; 71:119.
[34] Hatfield GR, Guo Y, Killinger WE, Andrejak A, Roubicek PM. Macromolecules 1993;26:6350.
[35] Warner S. J Elast Plast 1990;22:166.
[36] Niesten MCEJ, Gaymans RJ. J Appl Polym Sci 2001;81:1372.
[37] Niesten MCEJ, Gaymans RJ. Polymer 2001;42:6199.
[38] McLean RS, Sauer BB. J Polym Sci 1999;37:859.
[39] Sauer BB, McLean RS, Brill DJ, Londono DJ. Polym Mater Sci Engng 2001;85.
[40] Sauer BB, McLean RS, Brill DJ, Londono DJ. J Polym Sci, Part B: Polym Phys 2002;40:1727.
[41] Ward IM, editor. Structure and properties of oriented polymers. New York: Chapman & Hall; 1977. p. 44.
[42] Private Communication from Atofina via Sauer BB.
[43] Boublil H, Okroafor E, Belhoucine M, Rault J. Polym Engng Sci 1989;29(10):679.
[44] McCrum NG, Read BE, Williams G. Anelastic and dielectric effects in polymeric solids, 1st ed. New York: Dover Publications Inc; 1967. p. 561.
[45] Wunderlich B, Macromolecular physics, vol. 3. New York: Academic Press; 1980. p. 52.
[46] Cojazzi G, Ficher A, Garbuglio C, Malta V, Zannetti R. Makromol Chem 1973;168:289.
[47] Norholt MG, Tabor BJ, van Aartsen JJ. J Polym Sci 1972;A-2(10):191.
[48] Andrews EH. Proc R Soc Lond: A 1964;277:562.
[49] Oth JFM, Flory PJ. J Am Chem Soc 1958;80:1297.
[50] Desgrand JV. UK Patent No. 6334; 1832.
[51] Mertens A. UK Patent No. 9186; 1841.
[52] Baare F, Garelly JG. US Patent No. 24,691; 1859.
[53] Sheperd TL. US Patent 423,997; 1935.
[54] Lilaonitkul A, West JC, Cooper SL. J Macromol Sci Phys 1976; B12(4):563.
[55] Mody PC, Wilkes GL. J Appl Polym Sci 1981;26:2853.
[56] Alexander LE. X-ray diffraction methods in polymer science. New York: Wiley/Interscience; 1969.
[57] Tyagi D, Mcgrath JE, Wilkes GL. Polym Engng Sci 1986;26:1371.